

Identification of Low-Level Point Radiation Sources Using a Sensor Network

Nageswara S. V. Rao, Mallikarjun Shankar
Oak Ridge National Laboratory

Jren-Chit Chin, David K. Y. Yau
Purdue University

Srinivasan Srivathsan, S. Sitharama Iyengar
Louisiana State University

Yong Yang, Jennifer C. Hou
University of Illinois at Urban-Champaign

Abstract—Identification of a low-level point radiation source amidst background radiation is achieved by a network of radiation sensors using a two-step approach. Based on measurements from three sensors, the geometric difference triangulation method is used to estimate the location and strength of the source. Then a sequential probability ratio test based on current measurements and estimated parameters is employed to finally decide: (i) presence of a source with the estimated parameters, or (ii) absence of the source, or (iii) insufficiency of measurements to make a decision. This method achieves the specified levels of false alarm and missed detection probabilities, while ensuring close to minimal number of measurements to reach a decision. This method minimizes the ghost-source problem of the current estimation methods and achieves lower false alarm rate compared to current detection methods. This method is tested and demonstrated using: (a) simulations, and (b) a test-bed that utilizes the scaling properties of point radiation sources to emulate high intensity ones that cannot be easily and safely handled in experimentation.

Keywords and Phrases: Point radiation source, detection and localization, CUSUM, sequential probability ratio test.

I. INTRODUCTION

There has been an increasing interest in the identification of low-level radiation sources as a part of the defense strategy against dirty bomb scenarios. The ability to identify the signatures of such sources enables us to detect them before they are set-off, in particular while they are being transported or stored. In another scenario, such capability enables us to detect radiation traces and estimate their extent in “seemingly” conventional explosions so that first responders can be forewarned and suitably protected against such low-level yet very hazardous radiation. Typically, in both these scenarios the radiation levels could be low enough to appear as normal variations of the background radiation. This problem is particularly acute since the radiation measurements follow the Poisson process whose variance is of the same order as the radiation level itself. While long-term averages of low-level sources do result in elevated levels

and eventually be detected, our focus is on identifying them quickly to ensure fast response. In general, the area of detecting various radiation sources using individual sensors has been well established both in terms of devices and detection methods [14], [18], most of which are dedicated to single or co-located sensor systems. Recent advent of sensor network technologies, however, opened up the potential for improved detection, and also for the estimation of source parameters by utilizing measurements from multiple, geographically dispersed sensors, as reflected in several works (for example, [7], [10], [15], [19], [21], [22]).

Compared to the identification of high intensity radiation sources, detection and localization of low-level sources is difficult, particularly when the intensity levels are only marginally above background radiation levels. There are two major considerations:

- (a) **Varied Background Radiation:** The background radiation depends both on local natural and man-made sources and global sources such as cosmic rays, and hence may vary significantly from one deployment region to the other. If not carefully interpreted, such measurements may lead one to conclude “ghost” sources that potentially cause unnecessary response and panic.
- (b) **Probabilistic Radiation Measurements:** The radiation sources give rise to inherently probabilistic measurements. Typically the gamma radiation from point sources follows the Poisson distribution to a first order of approximation [14], [16].

The probabilistic nature combined with varied background radiation makes it hard to derive *a priori* thresholds needed by typical detection methods. Furthermore, the estimation of source location parameters is more complex compared to the usual triangulation methods developed for deterministic measurements. Nevertheless, the estimation can be made more effective when a network of sensors is employed, although many estimation problem still remain to be solved. In this paper,

we address above Item (a) by in-situ estimation of background radiation during an initial deployment phase of the network. We address Item (b) using a combination of geometric localization method and Sequential Probability Ratio Test (SPRT).

Probability ratio tests are typically employed in the *detection* problems to derive thresholds to achieve specified levels of false alarm rates and missed detection rates in both centralized [23] and distributed detection systems [25]. Such approach is described for the detection of radiation sources using single sensors in [9], [12], [18] (to name a few) and using copula methods in sensor networks in [22]. The estimation of the localization and strength of point radiation sources typically requires at least three sensors and is solved using least square methods in [11], [10], [17]. Typically, the *parameter estimation* methods implicitly assume that the measurements are due to the source and not the background, often, by utilizing a preceding detection step. Detection is not a major challenge for big sources that lead to large measurements, but for low-level sources these methods lead to “ghost” sources if the measurements correspond only to background. On the other hand, the detection can itself be made more accurate or robust if source parameters source are known in advance.

In this paper, we show that detection and estimation steps can reinforce each other using a two-step procedure for low-level radiation sources. We present a method for the *identification*, which subsumes detection and parameter estimation, of a point radiation source using a network of three sensors that provide radiation counts. In the first step, we utilize a geometric localization method to estimate the location of a real or ghost source from which we estimate its strength. Then using the estimated source parameters, we utilize SPRT to declare: (i) presence of source along with its estimated parameters, or (ii) absence of the source, or (iii) insufficiency of the collected measurements to make a decision. The localization method is derived by adapting the recently developed geometric difference-triangulation method to this case [20], and source strength is estimated using a linear combination of the estimates from individual sensors. The detection test is designed by estimating the background radiation of the given deployment and the source parameters to formulate SPRT based on Poisson point source model. Ghost sources, if estimated in the first step, will be rejected by SPRT since they do not lead to statistically consistent measurements. On the other hand, the estimated parameters enable us to formulate a more specific SPRT compared to detecting a general increase in radiation level; in particular, such SPRT provides the detection decision with least expected number of measurements. This approach is contract with

the detection followed by identification used in several tracking application [6], [5].

Testing of the identification methods for radiation sources poses pragmatic challenges since it is potentially hazardous and too expensive to deploy the radiation sources of all but minimal strengths. We exploit the simple product form of the radiation model to develop a scaled-down workbench that emulates larger deployments. In particular, we map the work bench with dimension of a few feet to emulate deployments of several hundred meters, and demonstrate the effectiveness of our method using real radiation sources.

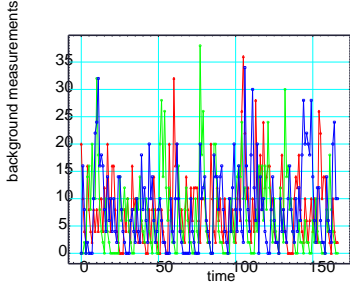
This paper is organized as follows. In Section II, we briefly describe the existing works on detection and estimation of radiation sources with a particular emphasis on sensor networks. We formulate the identification problem in Section III. We describe our solution to source parameter estimation problem in Section IV and the detection problem in Section V. We combine these results to develop our identification method in Section VI. We describe our simulation results in Sections IV and VI, and the test-bed results in VII.

II. RELATED WORKS

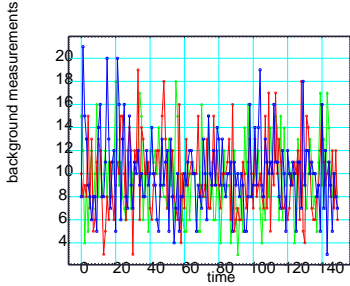
The detection and estimation of radiation sources of various kinds has been well-studied particularly using single sensors [14], [4]. The detection of radiation sources amidst background has been studied using SPRT for different scenarios such as long-term and portal monitoring [8], [12], [18]. These works do not directly address the source localization.

Utilization of networks of sensors for detecting and tracking radiation sources has been more recently addressed. For the detection of radioactive sources, linear arrangement of detectors have been considered in [19], [7], [15], and analysis of sensor network solutions was carried out for source moving in a linear mode in [21]. The detection of a point radiation source using a sensor network is addressed in [22] wherein the detection problem is decomposed into two parts such that individual sensor distributions are combined using a copula function that captures the correlations among sensors.

Typically, a detection method is used to assert the presence of a radiation source. Then a measurements from multiple sensors are used to estimate the parameters of the source. The problem of localization of a point radiation source has been addressed by [10], [17], [3]. Recursive and moving horizon non-linear least squares methods was proposed to track radioactive sources in [11]. Overall, the estimation methods assume that measurements corresponds to a source whereas the detection methods are most effective when the source parameters are accurately known.



(a) Measurements from RFTrax sensors



(b) Simulated Poisson variables with $\lambda = 10$.

Fig. 1. Background radiation counts show high variance.

III. PROBLEM FORMULATION

We consider the identification of a point radiation source S with unknown strength A_U expressed per unit time called the *source rate*, and located at an unknown location (x_u, y_u) . This source gives rise to an intensity of $I(x, y) = A_U/r^2$ at any point (x, y) , where $r = d((x_u, y_u), (x, y)) = \sqrt{(x_u - x)^2 + (y_u - y)^2}$. Lets $m_{i,1}, m_{i,2}, \dots, m_{i,n}$ be the sequence of radiation counts each measured per unit time at the sensor M_i at known location (x_i, y_i) , for $i = 1, 2, 3$. The radiation count due to the source observed at M_i per unit time is a Poisson random variable with parameter $\lambda = I(x_i, y_i)$ not accounting for the background radiation [14], [16].

Let $B(x, y)$ denote the background radiation strength expressed in unit time at (x, y) called the *background rate*, and the radiation count at sensor located at (x, y) is given by the Poisson random variable with parameter $B(x, y)$. The assumption of Poisson distribution of background measurements may not always be accurate since it could be a complex combination of various sources; we utilize this assumption for our main derivation and later account for the deviations. On the other hand, measurements of $I(x, y)$, being from a single point source, are more accurately characterized by the Poisson distribution. In either case, the measurements are statistically independent across the time units, and exhibit significant variation as shown in Figure 1.

We consider a monitoring area contained within the

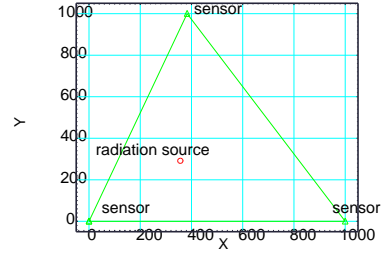


Fig. 2. Region monitored by three sensors that form acute triangle.

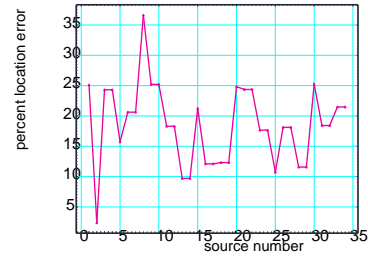


Fig. 3. Errors of location estimation method for 50 sources.

acute triangle formed by M_1, M_2, M_3 shown in Figure 2 to simplify the presentation of the localization method; however, this method is shown to work in general case [20], [27]. We are given three sequences of measurements collected within the same time-window at M_i , $i = 1, 2, 3$. The *Detection Problem* deals with inferring the presence of a source, and the *Estimation Problem* deals with estimating the location, that is localization, and also the source strength. The estimates of (x_u, y_u) and A_u are denoted by (\hat{x}_u, \hat{y}_u) and \hat{A}_u , respectively.

We characterize the solution by the *false alarm probability*, denoted by $P_{1,0}$, corresponding to declaring a presence of a source when none exist, and the *missed detection probability*, denoted by $P_{0,1}$, corresponding to declaring the presence of only the background radiation when a source is present in the monitoring region. We also characterize the performance of the solution method by *detection time* which is the size of time window or number of measurements needed to declare the source or just the background.

IV. SOURCE PARAMETER ESTIMATION

In this section, we first present a method to estimate (\hat{x}_u, \hat{y}_u) using an extension of the geometric triangulation method of [20], and then describe a linear fuser to estimate the source strength A_U .

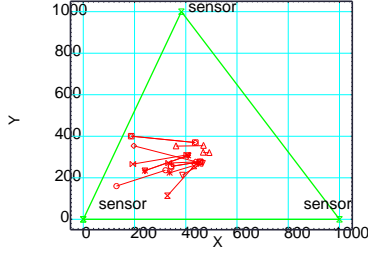


Fig. 4. Examples sources and their estimators joined by line segments.

A. Location Estimation

Let $m_{i;1}, m_{i;2}, \dots, m_{i;n_i}$ denote a sequence of n_i measurements collected by sensor M_i within a given time window. Using measurement counts from the sensors, we compute the mean of measurements at each sensor given by $\bar{m}_i = \frac{1}{n_i} \sum_{j=1}^{n_i} m_i^j$, $j = 1, 2, 3$, which is a measurement of A_U/r_i^2 , $r_i = \sqrt{(x_u - x_i)^2 + (y_u - y_i)^2}$. Thus, on the average we have $\frac{1}{2} \ln \left(\frac{E[m_i]}{E[m_k]} \right) = \ln r_i - \ln r_k$, which is the difference of distances from the source in ln-space. Let $\delta_{ik} = \frac{1}{2} \ln \left(\frac{\bar{m}_i}{\bar{m}_k} \right) = \ln r_i - \ln r_k$. Let L_{ik} denote the set of all points (x, y) in plane such that $\ln(r_i) - \ln(r_k) = \delta_{i,k}$. The geometric search method performs a binary search on L_{12} using $\delta_{1,3}$ as an objective function to locate a point (\hat{x}_u, \hat{y}_u) such that $|x_u - \hat{x}_u| \leq \epsilon$ and $|y_u - \hat{y}_u| \leq \epsilon$. The implementation details of this search algorithm can be found in [27].

We now establish the correctness of this binary search method by establishing that on L_{12} the function $\delta_{1,3}$ varies monotonically so that binary search can be supported¹. We show the monotonicity in ln-space for the scenario of Figure 2, and general case can be along the lines of [27]. Without loss of generality, we assume:

- (a) $S_1 = (0,0)$, $S_2 = (x_2, 0)$ and $S_3 = (x_3, y_3)$ such that $x_2 > 0$, $x_3 > 0$ and $y_3 > 0$. Also, $x_3 < x_2$.
- (b) Source is $S = (x, y)$ such that $x > 0$ and $y > 0$, and S is closer to S_1 than to S_2 and S_3 ; otherwise we can rotate the triangle and re-label the coordinates of sensors.

In general $S_i = (x_i, y_i)$, $i = 1, 2, 3$ and $d(S, S_i) = \sqrt{(x - x_i)^2 + (y - y_i)^2}$ and

$$\Delta(S_i, S_j) = \ln[d(S, S_i)] - \ln[d(S, S_j)].$$

Then we have

$$\frac{\partial d(S, S_i)}{\partial x} = \frac{(x - x_i)}{d(S, S_i)}$$

¹The monotonicity proof of [27] is valid for $\delta_{i,k} = r_i - r_k$ that is in actual distance space as opposed to ln-space here.

and

$$\frac{\partial d(S, S_i)}{\partial y} = \frac{(y - y_i)}{d(S, S_i)}.$$

By Item (b) we have $d(S, S_1) < d(S, S_2)$ and $d(S, S_1) < d(S, S_3)$.

The directional derivative of $\Delta(S_1, S_3)$ on the locus $\{(x, y) | \Delta(S_1, S_2) = \delta_{12}\}$, for any δ_{12} , is given by

$$\begin{aligned} & \nabla_{\Delta(S_1, S_2)} \Delta(S_1, S_3) \\ &= \left[\begin{array}{c} \frac{\partial \Delta(S_1, S_2)}{\partial x} \\ \frac{\partial \Delta(S_1, S_2)}{\partial y} \end{array} \right]^T \\ & \circ \frac{1}{\sqrt{\left(\frac{\partial \Delta(S_1, S_3)}{\partial x} \right)^2 + \left(\frac{\partial \Delta(S_1, S_3)}{\partial y} \right)^2}} \left[\begin{array}{c} \frac{\partial \Delta(S_1, S_3)}{\partial x} \\ \frac{\partial \Delta(S_1, S_3)}{\partial y} \end{array} \right] \\ &= \left[\begin{array}{c} \frac{x}{[d(S, S_1)]^2} - \frac{x - x_3}{[d(S, S_3)]^2} \\ \frac{y}{[d(S, S_1)]^2} - \frac{y - y_3}{[d(S, S_3)]^2} \end{array} \right]^T \\ & \circ \frac{1}{K} \left[\begin{array}{c} \frac{x}{[d(S, S_1)]^2} - \frac{x - x_2}{[d(S, S_2)]^2} \\ \frac{y}{[d(S, S_1)]^2} - \frac{y - y_2}{[d(S, S_2)]^2} \end{array} \right] \\ &= \left(\frac{x}{[d(S, S_1)]^2} - \frac{x - x_3}{[d(S, S_3)]^2} \right) \\ & \quad \left(\frac{x}{[d(S, S_1)]^2} - \frac{x - x_2}{[d(S, S_2)]^2} \right) \\ & \quad + \left(\frac{y}{[d(S, S_1)]^2} - \frac{y - y_3}{[d(S, S_3)]^2} \right) \\ & \quad \left(\frac{y}{[d(S, S_1)]^2} - \frac{y - y_2}{[d(S, S_2)]^2} \right) \end{aligned}$$

where $K = \frac{1}{\sqrt{\left(\frac{\partial \Delta(S_1, S_3)}{\partial x} \right)^2 + \left(\frac{\partial \Delta(S_1, S_3)}{\partial y} \right)^2}}$. Note that $x_2 > 0$, $x_3 > 0$ and $y_3 > 0$, and also $\frac{1}{d(S, S_1)} > \frac{1}{d(S, S_3)}$ and $\frac{1}{d(S, S_1)} > \frac{1}{d(S, S_2)}$. Then we conclude that $\nabla_{\Delta(S_1, S_2)} \Delta(S_1, S_3) > 0$ for all $x > 0$ and $y > 0$.

We now present simulation results to illustrate the performance of this method. Using 1000 randomly generated source locations with $A_U = 10^6$ and $B = 10$, and the errors in location estimation as a percent of distance between the sensors is shown in Figure 3. The average error is 20.07% for 1000 sources but the error has high variance due to the Poisson measurements. Some source locations and their estimators are shown in Figure 4, where a line-segment joins the source with its estimator.

We executed this algorithm when there is no source, that is, based only on background measurements with $B = 10, 100$ at the sensors. As shown in Figure 5, the ghost sources have been identified approximately near the centroid of the triangle formed by the sensors. In the next section we outline a method that utilizes the estimated source parameters in SPRT to decide on the presence of a real source, in particular rule out the ghost sources.

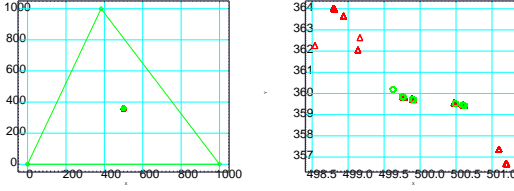


Fig. 5. Estimated ghost sources with expanded view on right.

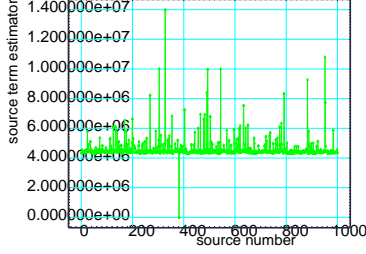


Fig. 6. Variation of source strength estimator for $A = 5 \times 10^5$.

B. Source Strength Estimation

Using the source location estimate (\hat{x}_u, \hat{y}_u) , we have three source strength estimates A_u given by $\hat{A}_i = \bar{m}_i \hat{r}_i^2$, for $i = 1, 2, 3$, where $\hat{r}_i = \sqrt{(x_i - \hat{x}_u)^2 + (y_i - \hat{y}_u)^2}$. We combine these three estimators using coefficients that are inversely proportional to their variance estimates. Since for Poisson process both the mean and variance are given by its parameter \bar{m}_i , more weight is given to estimates with lower variance. Thus, we have the following fused source strength estimator

$$\hat{A}_U = \sum_{i=1}^3 \hat{a}_i \hat{A}_i,$$

where $\hat{a}_i = \frac{1/\bar{m}_i}{\sum_{k=1}^3 1/\bar{m}_k}$. The signal strength estimates for

1000 simulated sources with $A = 5 \times 10^5$ and $B = 10$ are shown in Figure 6, and the average value of the fused source term estimator is shown in Figure 7.

V. SOURCE DETECTION

In this section we describe general SPRT for detecting the presence of source of intensity A against background intensity B .

A. SPRT Test

For measurements $m_{i;1}, m_{i;2}, \dots, m_{i;n}$ collected by sensor M_i within a given time window, by the definition of Poisson process we have

$$P(m_{i;j}) = \frac{C^{-m_{i;j}} e^{-C}}{m_{i;j}!},$$

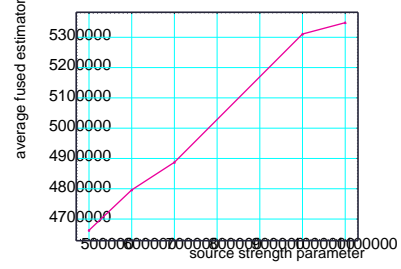


Fig. 7. Average fused source strength estimator.

with parameter $C = A + B$ if the source is present and $C = B$ if source is not present. Let H_C , for $C \in \{A, A + B\}$, denote the hypothesis that measurements correspond to the intensity level C . Now consider the likelihood function

$$l(m_{i;1}, m_{i;2}, \dots, m_{i;n} | H_C) = \prod_{j=1}^n \frac{C^{-m_{i;j}} e^{-C}}{m_{i;j}!},$$

wherein we utilized the statistical independence property of the measurements. We now consider the SPRT given by

$$L_{A,B;n} = \frac{l(m_{i;1}, m_{i;2}, \dots, m_{i;n} | H_{A+B})}{l(m_{i;1}, m_{i;2}, \dots, m_{i;n} | H_B)}$$

Then, we utilize SPRT [13] as follows:

- (i) If $L_{A,B;n} < \frac{P_{0,1}}{1-P_{1,0}}$ then declare H_B ;
- (ii) Else if $L_{A,B;n} > \frac{1-P_{0,1}}{P_{1,0}}$ then declare H_{A+B} ;
- (iii) Otherwise continue collecting additional measurements.

The following are the important properties of SPRT [13]:

- (a) The false alarm and missed detection rates of SPRT are given by $P_{1,0}$ and $P_{0,1}$, respectively.
- (b) Among all tests to decide between H_{A+B} and H_B with with given $P_{1,0}$ and $P_{0,1}$, SPRT minimizes $E[n|H_B]$ and $E[n|H_{A+B}]$ (see Theorem 2.4, [26] for example).

This test can be is compactly expressed as

$$\frac{P_{0,1}}{1-P_{1,0}} \leq L_{A,B;n} \leq \frac{1-P_{0,1}}{P_{1,0}},$$

which can be expressed in terms of the mean of measurements:

$$\begin{aligned} & \frac{\ln(P_{0,1}/(1-P_{1,0})) + nA}{\ln\left(\frac{A+B}{B}\right)} \\ & \leq \sum_{j=1}^n m_{i;j} \leq \\ & \frac{\ln((1-P_{0,1})/P_{1,0}) + nA}{\ln\left(\frac{A+B}{B}\right)}. \end{aligned}$$

Notice that the bounds on the average measurement $\bar{m}_i = \sum_{j=1}^n m_{i;j}$ will increase as a linear functions of the number of measurements.

This SPRT is derived under the assumption that measurements corresponding to both background and source radiation satisfy the the Poisson distribution. While point radiation sources follow such distribution, the complex nature of background radiation may not strictly satisfy such condition primarily because it could be a complex combination of multiple sources. In such case, the false alarm rate of this method can be different and can be approximated by the area under the distribution $P_B(x)$ for $x \leq \frac{\ln((1-P_{0,1})/P_{1,0})+nA}{\ln(\frac{A+B}{B})}$. This quantity can be estimated by utilizing the empirical distribution of background radiation at the sensor location. To address this issue, we present a more general detection method in the next section, whose optimal solution for the special case of Poisson background radiation is given by the above SPRT.

B. CUSUM Statistic

The CUSUM statistic CS_t at sensor M_i based on the measurements is given by [?]

$$CS_n = \sum_{j=1}^n (m_i^j - E[m_i]) \quad (1)$$

In absence of radiation source, CUSUM plot oscillates around value zero. However, when a radiation source S is present, the expected value of the sensor reading will increase due to the additive nature of the radiation counts, which leads to. to a positive slope in CUSUM plot over long period of time. The slope of the plot provide information about the strength of S , where steeper slope implies stronger S . Consider a threshold value τ such that a radiation source is detected when the CUSUM statistic CS_t exceeds the threshold. The performance of this heuristic is presented in the next subsection. The value of τ is chosen such that $\Pr\{CS_t \leq \tau | t = 1, 2, \dots\} \geq 1 - \alpha$, where α denotes the false alarm rate (or false positive rate). The value τ can be obtained empirically by deploying the sensors to the target locations and collect the radiation readings in a non-disturbed environment over a long period of time. This is known as the *training period* of the system. Lets N be the number of samples collected in the period, the cumulative probability distribution (CDF) of CUSUM for the sensor exposed to background radiation readings only $F_{CS}^B(x)$ can be estimated using the collected samples by

$$\hat{F}_{CS}^B(x) = \frac{|\{CS_t | CS_t \leq x, t = 1, 2, \dots, N\}|}{N} \quad (2)$$

Using theorems 3.7 and 4.3 in [24], the goodness of estimated false alarm rate α can be bounded by

$$\Pr\left\{\left|\hat{F}_{CS}^B(\tau) - F_{CS}^B(\tau)\right|\alpha\right\} \leq 8Ne^{1-\alpha^2N/8} \quad (3)$$

Equation 3 can be used as a guide-line to judge the length of training period required to reliably estimate the value of τ .

With threshold τ selected, the expected miss detection rate (or false negative rate) can be estimated as follow. Before we analyze the miss detection rate, lets derive the expected value of CUSUM statistic in a single radiation source scenario.

Theorem 5.1: Consider a radiation source S of strength A is introduced into the system at time k . The sensor at r distance away from S will report radiation readings of $E[s_t] = E[B] + A/r^2$ beginning at time $t = k + 1$. Prior to $k + 1$, the sensor reports readings of $E[s_t] = E[B]$. The expected value of CUSUM statistic of the given scenario is

$$E[CS_t] = \begin{cases} 0 & 1 \leq t \leq k \\ (t-k) \left(1 - \frac{1+t-k}{2w}\right) \frac{A}{r^2} & k+1 \leq t \leq k+w \\ \left(\frac{1}{2} - \frac{1}{2w}\right) \frac{Aw}{r^2} & t > k+w \end{cases} \quad (4)$$

Proof: For interval $1 \leq t \leq k$, $E[s_t] = E[B]$ because there is no detectable radiation source in the system. Thus, following from Equation ??, we have

$$\begin{aligned} E[CS_t] &= E\left[\sum_{i=1}^t \left(s_i - \frac{\sum_{j=\max(i-w,1)}^i s_j}{w}\right)\right] \\ &= \sum_{i=1}^t \left(E[B] - \frac{w \cdot E[B]}{w}\right) = 0 \end{aligned} \quad (5)$$

This completes the proof for the first case where $1 \leq t \leq k$. The equation for interval $k+1 \leq t \leq k+w$ can be proved by induction on t . Lets the following be the induction hypothesis: *Equation 6 is true for interval $k+1 \leq t \leq k+w$.*

$$E[CS_t] = (t-k) \left(1 - \frac{1+t-k}{2w}\right) \frac{A}{r^2} \quad (6)$$

Assumes Equation 6 is true for $t = k+m$ where $1 \leq m < w$. For the base case where $t = k+1$, the following is a result of Equation ??.

$$\begin{aligned} E[CS_{k+1}] &= E[s_{k+1}] - \left(\frac{w-1}{w}E[B] + \frac{1}{w}E[s_{k+1}]\right) \\ &+ E\left[\sum_{i=1}^k \left(s_i - \frac{\sum_{j=\max(i-w,1)}^i s_j}{w}\right)\right] \end{aligned}$$

Using the result of Equation 5 and substituting $E[s_{k+1}] = A/r^2 + E[B]$, the above equation reduces to

$$E[CS_{k+1}] = \left(1 - \frac{1}{w}\right) \frac{A}{r^2}$$

Substituting $t = k + 1$ into Equation 6 yields identical equation as the above. This proves the base case.

By induction on t , we prove $t = k + m + 1$ is true in the following. As the source remains constant after introduced to the system, $E[s_{k+m+1}] = E[B] + A/r^2$. From Equation ??, we have

$$\begin{aligned} E[CS_{k+m+1}] &= E[s_{k+m+1}] + E[CS_{k+m}] \\ &\quad - \left(\frac{w-m-1}{w} E[B] + \frac{m+1}{w} E[s_{k+m+1}] \right) \\ &= \left(1 - \frac{m+1}{w} \right) \frac{A}{r^2} + E[CS_{k+m}] \end{aligned}$$

By assumption, substitute $E[CS_{k+m}]$ in the above equation with Equation 6 and thus yield the following.

$$\begin{aligned} E[CS_{k+m+1}] &= \left(1 - \frac{m+1}{w} \right) \frac{A}{r^2} + m \left(1 - \frac{1+m}{2w} \right) \frac{A}{r^2} \\ &= \left[m + 1 - \frac{m+1}{w} - \frac{m(m+1)}{2w} \right] \frac{A}{r^2} \\ &= (m + 1) \left(1 - \frac{2+m}{2w} \right) \frac{A}{r^2} \end{aligned} \quad (7)$$

Substituting $t = k + m + 1$ into Equation 6 yields identical equation as above, thus the induction hypothesis holds.

Similar for interval $t > k + w$, the expected value of s_t equals to g_t as all samples in the moving average window are sampled after the radiation source introduced into the system. In other word, the system has adapted to the new environment. For $t = k + w + 1$, the following is a result of Equation ??.

$$\begin{aligned} E[CS_{k+w+1}] &= E[CS_{k+w}] + E[s_{k+w+1}] \\ &\quad - \left(\frac{w-1}{w} \cdot \frac{A}{r^2} + \frac{1}{w} E[s_{k+w+1}] \right) \\ &= E[CS_{k+w}] = \left(\frac{1}{2} - \frac{1}{2w} \right) \frac{Aw}{r^2} \end{aligned}$$

As $E[s_t - g_t] = 0$, we have $E[CS_t] = E[CS_{t-1}]$ for all $t > k + w$ following Equation ?. Hence, we obtain Equation 4. ■

Using Theorem 5.1, the detection time t_D in terms of number of samples can be obtain by the following.

$$t_D = \arg \min_t \{ E[CS_t] > \tau \}$$

and the miss detection rate is as the following.

$$P_D = \Pr \left\{ \left(\frac{1}{2} - \frac{1}{2w} \right) \frac{Aw}{r^2} < \tau \mid A, r, w, \tau \right\}$$

VI. IDENTIFICATION METHOD

We now combine source parameter estimation and SPRT methods of previous sections to develop an identification method. Initially the background radiation measurements are collected by each sensor and averaged to estimate the local background radiation level \hat{B}_i . Then, the network is put into monitoring mode, and the identification of the source is achieved using the following procedure:

- (i) Using the readings from three sensors, we estimate the source location (x_u, y_u) and compute source intensity estimate \hat{A}_U .

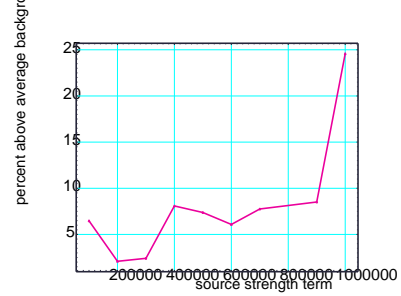


Fig. 8. Percent above background level due to sources with $A = 2 \times 10^5, 5 \times 10^5, 6 \times 10^5, 7^5, 10 \times 10^5$.

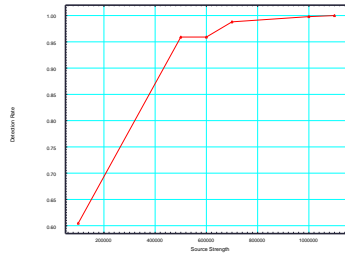
- (ii) We utilize SPRT $L_{\hat{A}/\hat{r}_i, \hat{B}_i; n}$ to conclude $H_{\hat{A}/\hat{r}_i + \hat{B}_i}$ versus $H_{\hat{B}_i}$ at sensor i . We declare $H_{\hat{A}/\hat{r}_i + \hat{B}_i}$ and $H_{\hat{B}_i}$ if and only if the respective threshold conditions are satisfied at two or three sensors M_i , $i = 1, 2, 3$. Otherwise measurement collection will be continued.

Initially, the default hypothesis is $H_{\hat{B}_i}$, and is changed only if $H_{\hat{A}/\hat{r}_i + \hat{B}_i}$ is declared by a majority of sensors.

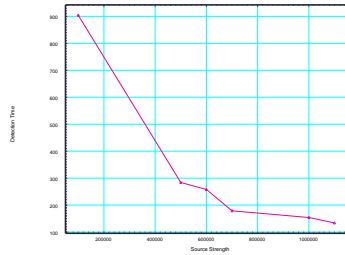
This procedure has a minimum false alarm rate of the two or three sensors that declared $H_{\hat{A}/\hat{r}_i + \hat{B}_i}$ to assert the presence of a source. This method was tested using 1000 randomly generated sources with $A = 10^5, 5 \times 10^5, 6 \times 10^5, 7^5, 10 \times 10^5$. The average increase of the radiation level over the background at these source strength is below 10% for most of them as shown in Figure 8, but over a short time-period the variation due to background could be 100%. The detection rates for various source terms are shown in Figure 9(a) for $P_{0,1} = P_{1,0} = 0.1$, which is 100% for $A = 10^6$ or higher. Note that the detection rate was higher than 95% for $A = 4 \times 10^5$ or higher even though the average increase in the radiation level at the sensor locations is within the range [5, 10] percent.

The detection times are shown Figure 9(b) which shows a decreasing trend with increasing A - as expected it is easier to detect sources with higher strengths. The average detection time was less than 300 for $A = 4 \times 10^5$ or higher even though the average increase in the radiation level at the sensor locations is within [5 - 10] percent. However, the actual detection times showed significant variation as shown in Figure 10(a) for the case $A = 10^6$.

When no source is present, the ghost source will likely be located at the centroid of the triangle formed by the sensors. But the corresponding high threshold for $H_{\hat{A}/\hat{r}_i + \hat{B}_i}$ in Step (ii) will not be met, and hence the false alarm will be cleared. In our simulations with 10000 measurements with $B = 10, 100$, this method did not generate a single false alarm. However, the average detection time is 1309 and 159 for $B = 10$ and $B = 100$,

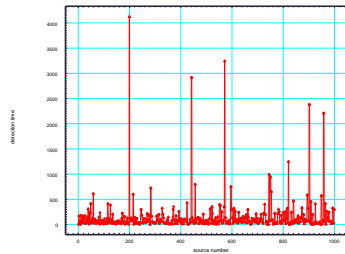


(a) average detection rate

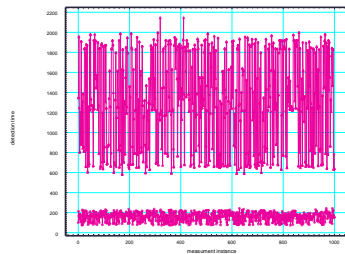


(b) average detection time

Fig. 9. Performance of identification method.



(a) source with $A = 10^6$ and background with $B = 10$



(b) no source and background with $B = 10, 100$

Fig. 10. Detection times for the source and background

respectively, but their the actual detection times have a high variation as shown in Figure 10(b).

It is instructive to compare this method with two exiting approaches:

- (a) Compared to existing detection methods, this method has a more focused goal of point source rather than general increase in measurements. SPRT in Step (ii) guarantees that it is uniformly most powerful test at given false alarm rate in terms of maximizing detection rate and minimizing the detection time.
- (b) Compared to the estimation methods, this ghost source phenomenon is strictly controlled by the false alarm probability. Furthermore, the in-situ estimation of background radiation levels makes it sensitive to variations in the background radiation across the deployment region.
- (c) Compared to existing methods that utilize a detection method followed by estimation, the present method achieves lower false alarm rate since SPRT in Step (ii) does not have to account for all possible source levels.

VII. EXPERIMENTAL RESULTS

A. Test-bed System Setup

We setup three radiation sensing test-beds at (i) SensorNet Laboratory at Oak Ridge National Laboratory (ORNL), (ii) Purdue University, and (iii) University of Illinois at Urbana-Champaign. All three test-beds have similar configuration except the number of radiation sensors available. Figure 12 shows the equipment layout of the test-bed for the experiments. The components of the test-bed include a collection of Rad-CZT radiation sensors by RFTrax Inc. [1], a Sensornet node, and a wireless router. The SensorNet node (see Figure 11) is a hardware platform developed in ORNL intended to allow a wide variety of sensors to be monitored and managed over a nation-wide distributed network. The wireless router allows communication among multiple Sensornet nodes as well as a Ethernet switch for connecting the sensors. The radiation sensors (RS485 device) connect to the Sensornet node via iServer [2]. The iServer proxies the RS485/232 interface (the radiation sensors in this case) to Ethernet interface and thus provide access to the sensors via TCP/IP. The Sensornet node runs standard Linux operating system (Fedora Core) and Sensornet node software developed by ORNL. The software is configured to poll each sensor in 4 second interval and stores the sensor readings in a MySQL database. In addition of storing the sensor readings, we augmented the Sensornet node to send the sensor data to a workstation in real-time for on-line analysis.

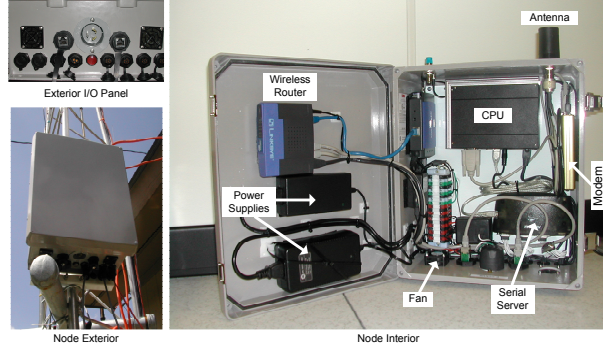


Fig. 11. The Sensornet node hardware.

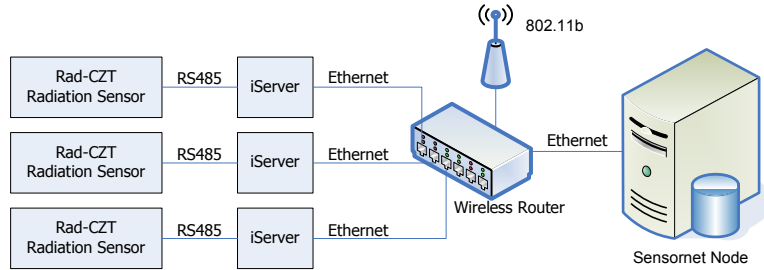


Fig. 12. Radiation Sensing Test-bed Equipment Setup.

Day 1			
Sensor	Mean	Stdev	#Samples
RFTrax1	7.80	7.12	9900
RFTrax2	7.46	7.01	9900
RFTrax3	8.08	7.46	9900
Day 2			
Sensor	Mean	Stdev	#Samples
RFTrax1	7.62	7.13	9900
RFTrax2	7.54	7.07	9900
RFTrax3	8.00	7.30	9900

TABLE I
STATISTIC OF BACKGROUND RADIATION IN SENSORNET LAB.

B. Background Radiation Profile

The three radiation sensors were activated to collect radiation readings from on two different days. All total 9,900 samples were collected at 4 second intervals. Figure 13 shows the distribution of background radiation as reported. The statistic of the data collected is reported in Table I.

We performed z-test for comparing the means of two independent samples to compare the radiation counts at three sensors of the test-bed. The test result shows that the probability of two sensors producing the same mean value is 0.63% at the maximum. In other words, the mean values are different with 99.37% level of significant even the sensors are located within 2 feet apart to each other at maximum. We conclude that each sensor requires separate background radiation profile.

C. Radiation Sensor Emulator

The background radiation distribution as shown in Figure 13 can be used directly in simulation application. However, we can achieve similar result by emulating the radiation sensor. This approach provides us better control on the radiation level in simulation. The RFTrax Rad-CZT radiation sensors being used in the test-bed performs filtering to the particle counts data collected. In particular, the filter approximates the traditional exponential filtering. We approximate the background radiation particles arrive at the sensor by a Poisson variable with $\lambda = E[B]$. Then, we emulate the sensor firmware to perform particle counting and exponential filtering. Figure 14 shows the distribution of actual background radiation and approximation using the method described. The approximation achieve chi-square statistic of $\chi^2 = 179.95$.

D. CUSUM Detection

We performed Monte Carlo simulation to determine the false alarm rate as well as detection time of CUSUM. We setup a simulation environment where a virtual RFTrax radiation sensor is receiving P Poisson (7.80) radiation particle every minute (background radiation rate) for time $1 \leq t \leq k$ where $k = 1296000\text{sec}$ or 15 days. For time $t > k$, the virtual RFTrax radiation sensor is receiving P Poisson (λ) radiation particle every minute for $\lambda = 10, 20, 30, 40, 50$. The CUSUM alarm

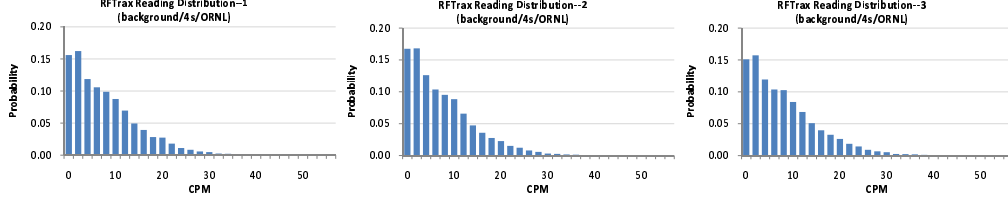


Fig. 13. Background radiation distribution in ORNL Sensornet Laboratory.

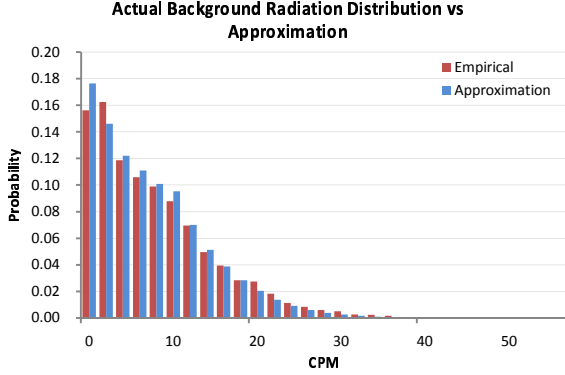


Fig. 14. Actual background radiation reading collected on day 1 versus approximation by emulation

threshold is set to $\tau = 100, 200, \dots, 1000$. The sensor was configured to perform exponential filtering with filter depth of 6 samples and was being polled every 4 seconds. The simulation is repeated for $N = 2000$ times and the average false alarm rate and detection time is computed.

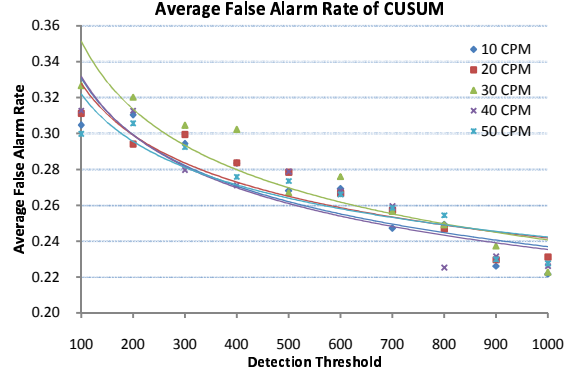
Because there is no radiation source presence for $1 \leq t \leq k$, all alarm signaled represent false alarms. We compute the false alarm rate P_F as the following.

$$P_F = \frac{|\{CS_t | CS_t \geq \tau, 1 \leq i \leq k\}|}{k} \quad (8)$$

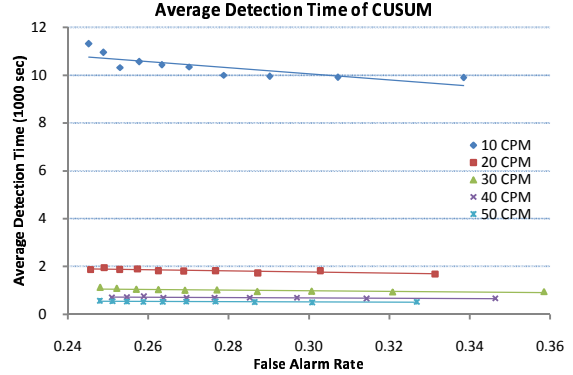
The sensor is picking up readings with the radiation source presence at time $t > k$. The detection time is defined as the interval since the radiation source is first presence k until CS_t first exceed the threshold τ after the radiation source is presence. Mathematically, the detection time t_d is defined as

$$t_d = \arg \min_t \{CS_t \geq \tau | t > k\} - k \quad (9)$$

Figure 15 shows the simulation result of CUSUM detection. We found that the average false alarm rate achieved decreases sub-linearly with respect to the detection threshold. In fact, it is very hard to reduce the false alarm rate lower than 23%. Unlike the decreasing trend of miss detection rate in Neyman-Pearson test, the average detection time of CUSUM highly dependent on the intensity of the radiation source and less dependent on the false alarm rate.



(a) Average false alarm rate.

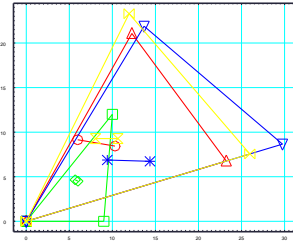


(b) Average detection time.

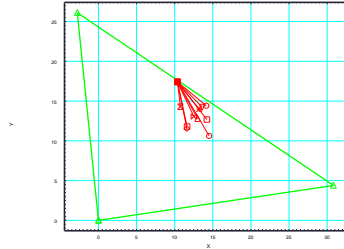
Fig. 15. Simulation result of CUSUM.

E. Localization Method

A Cs-137 radiation source of strength 0.95μ Curies was used on a table top with RFTrax RAD-CZT sensors to collect measurements to estimate the locations of the source using the difference triangulation method described in Section IV-A. In Figure 16(a) we show examples with different source locations and their estimates, and in Figure 16(b) we show repeated measurement with same source and sensor locations. The performance of this method is summarized in Table II wherein top six rows correspond to different sensor and/or source locations and the other rows correspond to repeated measurements with same sensor and source locations. The errors in the location estimates are plotted in Figure 17 with an average error of 4.87 inches. When no source



(a) different sensor and source locations



(b) different measurements with same source and sensor locations

Fig. 16. Example of localization of Cs-137 radiation source.

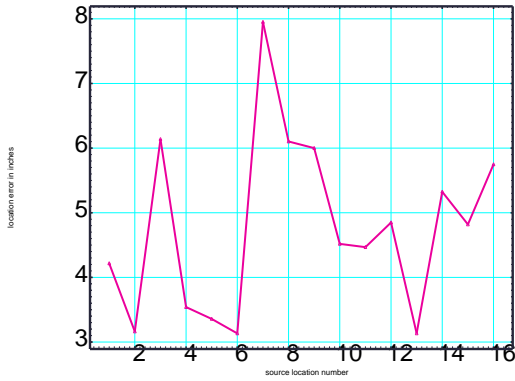
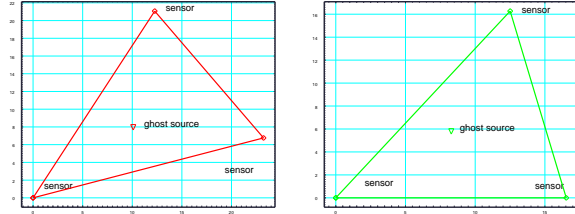


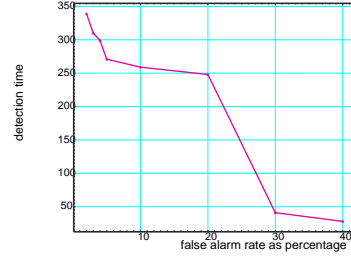
Fig. 17. Plot of location estimation errors corresponding to Table II.

is present the localization method returns ghost sources shown in two examples in Fig. 18(a).

In both cases, the SPRT declared that no radiation source is present, and the number of measurements needed for making this varied from 28 to 339 are the false alarm rate is reduced from 40% to 2% as shown in Fig. 18(b).



(a) ghost sources



(b) detection time vs. false alarm rate.

Fig. 18. Ghost sources computed and rejected.

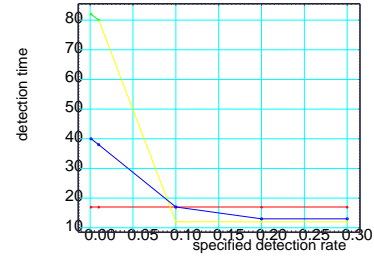


Fig. 19. A case that missed the detection.

F. Identification Method

The identification method rejected the ghost sources computed based on background reading shown in Figure 18 in both cases but the decision time was a function of false alarm rate $P_{1,0}$. When $P_{1,0} = 0.001$, detection time was 339 but was reduced to 28 when false alarm rate is reduced from 40% to 2% as shown in Fig. 18(b).

The source was present detection rate varied based on τ the number of initial measurements used before SPRT was applied for experiments. For the case in Table II with $P_{0,1} = 0.1$, for $\tau \leq 10$ the false alarm rate is 0.3, improved to 0.1 when $\tau = 25$, and reached 0 when $\tau = 75$. We now examine the configuration that missed detection for $\tau = 25$, corresponding to row five of Table II, in detail by varying $P_{0,1}$ using four repeated measurement sets. The detection times are shown in 19 which take lower values as we increased

TABLE II
EXPERIMENTS WITH REAL RADIATION SOURCE (0.95 μ CURIES)

Sensor1 (inches)	Sensor2 (inches)	Sensor3 (inches)	Radiation Source (X-Coord)	Radiation Source (Y-Coord)	Estimated Source (X-Coord)	Estimated Source (Y-Coord)	Error (inches)
(0.000000,0.000000)	(30.602287,0.000000)	(13.675448,19.949490)	13.405861	4.386448	17.115189	2.381002	4.216743
(0.000000,0.000000)	(30.602287,0.000000)	(13.593755,18.952833)	13.405861	4.386448	15.135843	1.739075	3.162503
(0.000000,0.000000)	(22.247314,3.171276)	(0.580224,24.782320)	9.634589	16.085903	8.543552	10.045546	6.138101
(0.000000,0.000000)	(21.416813,3.052891)	(-0.777120,24.122522)	8.651486	14.781301	10.081639	11.542296	3.540690
(0.000000,0.000000)	(20.600409,2.936517)	(-2.147295,23.407032)	7.679018	13.477128	9.818337	10.890409	3.356755
(0.000000,0.000000)	(30.833141,4.395156)	(-2.780083,26.101171)	10.365036	17.406164	10.743387	14.296099	3.132995
(0.000000,0.000000)	(30.833141,4.395156)	(-2.780083,26.101171)	10.365036	17.406164	14.519333	10.625864	7.951770
(0.000000,0.000000)	(30.833141,4.395156)	(-2.780083,26.101171)	10.365036	17.406164	14.225346	12.679550	6.102694
(0.000000,0.000000)	(30.833141,4.395156)	(-2.780083,26.101171)	10.365036	17.406164	11.587751	11.531683	6.000380
(0.000000,0.000000)	(30.833141,4.395156)	(-2.780083,26.101171)	10.365036	17.406164	13.601833	14.253601	4.518353
(0.000000,0.000000)	(30.833141,4.395156)	(-2.780083,26.101171)	10.365036	17.406164	13.222704	13.971645	4.467906
(0.000000,0.000000)	(30.833141,4.395156)	(-2.780083,26.101171)	10.365036	17.406164	12.517107	13.061058	4.848851
(0.000000,0.000000)	(30.833141,4.395156)	(-2.780083,26.101171)	10.365036	17.406164	10.743387	14.296099	3.132995
(0.000000,0.000000)	(30.833141,4.395156)	(-2.780083,26.101171)	10.365036	17.406164	13.006941	12.783309	5.324514
(0.000000,0.000000)	(30.833141,4.395156)	(-2.780083,26.101171)	10.365036	17.406164	14.143291	14.415342	4.818738
(0.000000,0.000000)	(30.833141,4.395156)	(-2.780083,26.101171)	10.365036	17.406164	11.625648	11.797838	5.748257

$P_{0,1} = 0.001, 0.01, 0.1, 0.2, 0.3$. Among the four separate measurement sets, only one set missed detecting the source for $P_{1,0} = 0.1, 0.2, 0.3$.

VIII. CONCLUSIONS

We addressed the identification of a low-level point radiation source amidst background radiations achieved by a network of radiation counters using a two-step approach. Based on measurements from three sensors, the geometric difference triangulation method is used to estimate the location and strength of the source. Then a sequential probability ratio test based on current measurements and estimated parameters is employed to finally decide: (i) the presence of a source with the estimated parameters, or (ii) the absence of the source, or (iii) insufficiency of measurements to make a decision. This method achieves the specified levels of false alarm and missed detection probabilities, while ensuring close to minimal number of measurements to reach a decision. This method minimizes the ghost-source problem of the current estimation methods and achieves lower false alarm rate compared to current detection methods. This method is tested and demonstrated using: (a) simulations, and (b) a test-bed that utilizes the scaling properties of point radiation sources to emulate high intensity ones that cannot be easily handled in practice.

There several potential directions for future research. First the localization method can be extended to networks involving more than 3 perhaps large number of sensors. More experimental validation would be useful by using sources of multiple strengths. The estimation of the source strength can be improved using a training step wherein the fuser can be calibrated for example by determining offset and a scale factor.

REFERENCES

- [1] <http://www.rfrax.com/radczt.html>.
- [2] <http://www.newportus.com/Products/ProdFam/iServer.htm>.
- [3] D. N. Anderson, D. C. Stromswold, S. C. Wunschel, A. J. Peurrung, and R. R. Hansen. Detection and location of Gamma-Ray sources with a modulating coded mask. *Technometrics*, 48(2):252–261, 2006.
- [4] Daniel E. Archer, Brock R. Beauchamp, G. Joseph Mauger, Karl E. Nelson, Michael B. Mercer, David C. Pletcher, Vincent J. Riot, James L. Schek, and David A. Knapp. Adaptable radiation monitoring system and method, 2006. U.S. Patent 7,064,336 B2.
- [5] Y. Bar-Shalom and X. R. Li. *Multitarget-Multisensor Tracking: Principles and Techniques*. YBS Publishing, 1995.
- [6] S. Blackman and R. Popoli. *Design and Analysis of Modern Tracking Systems*. Artech House, Boston, 1999.
- [7] S. M. Brennan, A. M. Mielke, and D. C. Torney. Radiation detection with distributed sensor networks. *IEEE Computer*, pages 57–59, August 2004.
- [8] P. E. Fehlau. Comparing a recursive digital filter with the moving-average and sequential probability-ratio detection methods for SNM portal monitors. *IEEE Transactions on Nuclear Science*, 40(2):143–146, 1993.
- [9] P. E. Fehlau. Comparing a recursive digital filter with the moving-average and sequential probability-ratio detection methods for SNM portal monitors. *IEEE Transactions on Nuclear Science*, 40(2):143–146, 1993.
- [10] A. Gunatilaka, B. Ristic, and R. Gailis. On localisation of a radiological point source. In *International Conference on Information, Decision and Control*. 2007.
- [11] J. W. Howse, L. O. Ticknor, and K. R. Muske. Least squares estimation techniques for position tracking of radioactive sources. *Automatica*, 37:1727–1737, 2001.
- [12] K. D. Jarman, L. E. Smith, and D. K. Carlson. Sequential probability ratio test for long-term radiation monitoring. *IEEE Transactions on Nuclear Science*, 51(4):1662–1666, 2004.
- [13] N. L. Johnson. Sequential analysis: A survey. *Journal of Royal Statistical Society, Series A*, 124(3):372–411, 1961.
- [14] G. F. Knoll. *Radiation Detection and Measurement*. John Wiley, 2000.
- [15] A. Mielke, D. Jackson, S. M. Brennan, M. C. Smith, D. C. Torney, A. B. Maccabe, and J.F. Karlin. Radiation detection with distributed sensor networks. In *SPIE Defense and Security Proceedings*, 2005.
- [16] D. Mihalas and B. W. Mihalas. *Foundations of Radiation Hydrodynamics*. Courier Dover Publications, 2000.

- [17] M. Morelande, B. Ristic, and A. Gunatilaka. Detection and parameter estimation of multiple radioactive sources. In *International Conference on Information Fusion*. 2007.
- [18] Karl E. Nelson, John D. Valentine, and Brock R. Beauchamp. Radiation detection method and system using the sequential probability ratio test, 2007. U.S. Patent 7,244,930 B2.
- [19] R. J. Nemzek, J. S. Dreicer, D. C. Torney, and T. T. Warnock. Distributed sensor networks for detection of mobile radioactive sources. *IEEE Transactions on Nuclear Science*, 51(4):1693–1700, 2004.
- [20] N. S. V. Rao, X. Xu, and S. Sahni. A computational geometric method for dtoa triangulation. In *International Conference on Information Fusion*, 2007.
- [21] D. L. Stephens and A. J. Peurrung. Detection of moving radioactive sources using sensor networks. *IEEE Transactions on Nuclear Science*, 51(5):2273–2278, 2004.
- [22] A. Sundaresan, P. K. Varshney, and N. S. V. Rao. Distributed detection of a nuclear radioactive source using fusion of correlated decisions. In *International Conference on Information Fusion*, 2007.
- [23] H. L. Van Trees. *Detection, Estimation and Modulation Theory, Part I*. John Wiley, 1968.
- [24] V. N. Vapnik. *The Nature of Statistical Learning Theory*. Springer-Verlag, New York, 1995.
- [25] P. K. Varshney. *Distributed Detection and Data Fusion*. Springer-Verlag, 1997.
- [26] G. B. Wetherill. *Sequential Methods in Statistics*. Methuen and Co., 1966.
- [27] X. Xu, N. S. V. Rao, and S. Sahni. A computational geometry method for localization using difference of distances. 2007. manuscript.